

CrystEngComm

Accepted Manuscript



This is an *Accepted Manuscript*, which has been through the Royal Society of Chemistry peer review process and has been accepted for publication.

Accepted Manuscripts are published online shortly after acceptance, before technical editing, formatting and proof reading. Using this free service, authors can make their results available to the community, in citable form, before we publish the edited article. We will replace this *Accepted Manuscript* with the edited and formatted *Advance Article* as soon as it is available.

You can find more information about *Accepted Manuscripts* in the [Information for Authors](#).

Please note that technical editing may introduce minor changes to the text and/or graphics, which may alter content. The journal's standard [Terms & Conditions](#) and the [Ethical guidelines](#) still apply. In no event shall the Royal Society of Chemistry be held responsible for any errors or omissions in this *Accepted Manuscript* or any consequences arising from the use of any information it contains.

Cite this: DOI: 10.1039/c0xx00000x

www.rsc.org/xxxxxx

ARTICLE TYPE

A Versatile Synthetic Approach for the Synthesis of CoO, Co_xC, and Co based Nanocomposites: Tuning Kinetics and Crystal Phase with Different Polyhydric Alcohols

Zachary J. Huba and Everett E. Carpenter*

Received (in XXX, XXX) Xth XXXXXXXXX 20XX, Accepted Xth XXXXXXXXX 20XX
DOI: 10.1039/b000000x

The solution synthesis of magnetic nanoparticles allows for precise control of a particle's shape, size, and crystal phase on the nanoscale, key parameters in tuning the intrinsic magnetic properties of nanoparticles. In this study, we investigate the role of polyhydric alcohols for the solution synthesis of cobalt carbide nanoparticles, a newly discovered hard ferromagnetic material. The oxidative stability of the polyhydric alcohol at reaction temperatures plays a significant role in the kinetics of carbide formation, as well as the phase produced (Co₂C vs. Co₃C). By tuning the oxidation rate of the polyhydric alcohol, composites of CoO, Co_xC, and Co phases can be produced, allowing for magnetic composites comprised of anti ferromagnetic, hard ferromagnetic and soft ferromagnetic phases.

Introduction

Cobalt and cobalt oxide nanomaterials have many industrial uses and possess interesting magnetic and catalytic properties.^{1, 2} Metallic cobalt has the second highest magnetization value of any pure metal and can be used as a soft or hard ferromagnetic material.²⁻⁵ Hard ferromagnetic cobalt phases exist for binary alloys with lanthanides (e.g. Sm) and cobalt carbide phases.^{2, 6-8} Solution processed Co_xC nanomaterials can have magnetizations as high as 70 emu/g with coercivities as large as 3 kOe.⁶ However, the mechanism for the solution processing of Co_xC nanomaterials requires an increased understanding, in order to optimize their magnetic properties.

The solution based synthesis of Co_xC nanomaterials utilizes a synthetic technique known as the polyol process.⁶⁻⁸ In the polyol process, a metal salt is heated in a polyhydric alcohol or polyol.⁹ At temperatures near its boiling point, the polyol acts as a reducing agent and capping agent to produce metal nanoparticles. However, cobalt carbide phases (Co₂C and Co₃C) can be formed when using a high boiling point polyol, like tetraethylene glycol.⁶⁻⁸ The inclusion of C atoms into the Co metal structures causes Co₂C and Co₃C to crystallize with orthorhombic structures. This change in crystal structure causes the Co_xC phases to possess higher coercivity, but lower magnetization values when compared to Co metal.⁸ Hence, the magnetic properties (magnetization and coercivity) for nanocomposites comprised of Co metal and Co_xC phases can be tuned by varying the phase ratio of Co and Co_xC.⁸

In a previous report, we have demonstrated the ability to control the crystal phase in polyol synthesized Co_xC and Co nanocomposites.^{7, 8} This control was facilitated by varying the amount of base added, which can act to increase the oxidation kinetics of the tetraethylene glycol.¹⁰⁻¹⁴ To further study the effect

of glycol oxidation towards the formation of cobalt crystal phase formation, we compare the reactivity of tetraethylene glycol and triethylene glycol as solvents and reducing agents. It is demonstrated, that by varying the glycol and amount of glycol in the reaction system, the kinetics of reduction and carbide formation can be controlled. Hence by selecting the appropriate synthesis parameters, nanocomposites comprised of Co₂C, Co₃C, Co metal, and CoO can be produced. This allows for a versatile one pot synthetic approach for the formation of Co based nanomaterials with varying and controllable magnetic properties.

Experimental Section

Synthesis

Tetraethylene Glycol (4-EG) and Triethylene Glycol (3-EG) were dried through the addition of 3 Å molecular sieves to the storage bottles to remove any accumulated water. All reactions were carried out with a final volume of 25 mL. In a typical reaction, a mixture of oleylamine and 3-EG or 4-EG was degassed for 5 minutes with N₂ at room temperature. The oleylamine and glycol mixture was then heated to 300 °C, under N₂ and mechanical stirring. The heating process took 20 minutes on average from room temperature to 300 °C. Once at 300 °C, 250 mg (0.86 mmol) of Co(NO₃)₂•6H₂O was added as a dry powder to the oleylamine and glycol mixture. The reaction was then kept at 300 °C for the desired reaction time. Upon completion of the reaction, the solution was allowed to cool to room temperature still under N₂ and mechanical stirring. The cooling process took 30 minutes. Once at room temperature the reaction solution was centrifuged for 5 minutes at 5000 rpm, to separate the particles from the supernatant. The collected particles were then rinsed and sonicated with a mixture of hexanes and acetone and then centrifuged to collect the particles from the

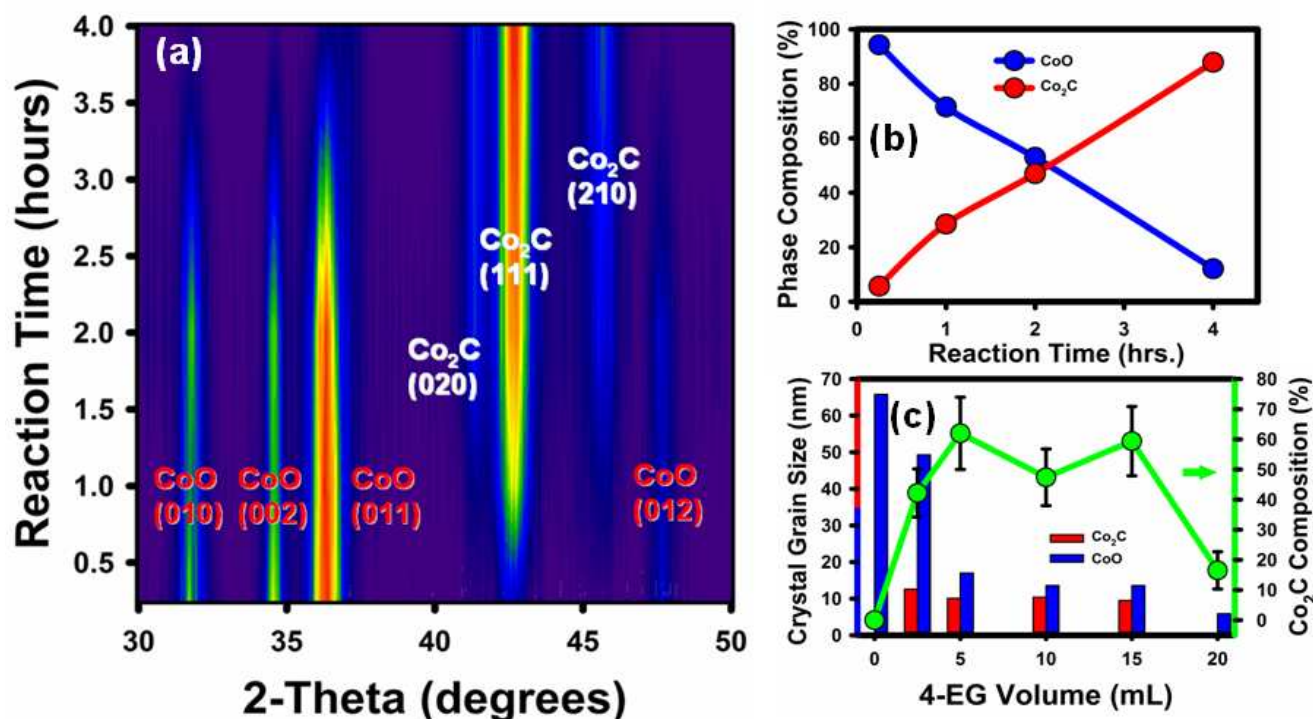


Figure 1. (a) Contour Plot showing diffraction intensities between 30° and 50° as a function of time for reaction using 10 mL of 4-EG and 15 mL oleylamine. (b) Line graph showing the change in CoO and Co₂C crystalline components as a function of time. (c) Crystal grain sizes and Co₂C composition values as a function of 4-EG volume. Individual scans are shown in Supplemental Information (S1 and S10)

5 wash solution. This process was repeated numerous times. Once clean, the particles were dried in a vacuum oven for an hour at room temperature.

Characterization

Crystal structure analysis was carried out using a PANalytical
 10 X'Pert Pro MPD diffractometer under Cu K α ($\lambda=1.5418$ Å). Analysis of collected X-Ray Diffraction (XRD) scans was performed using X'Pert Highscore analysis software. Phase composition and peak widths were determined as a result of Reitveld refinement using space groups and lattice parameters
 15 from literature.¹⁵ Crystal grain size was determined using the Scherrer Calculator in X'pert Highscore. Transmission electron imaging and analysis was conducted on a Zeiss Libra120 with an accelerating voltage of 120 kV. Elemental mapping of cobalt was conducted using Electron Energy Loss Spectroscopy (EELS) at the L-edge. Raman spectra were collected on a Thermo Scientific DXR Smart Raman using an excitation wavelength of 532 nm. Fourier Transform Infrared Spectroscopy (FT-IR) spectra were obtained on a Nicolet 6700 spectrometer, utilizing a SmartATR (Attenuated Total Reflectance mode) attachment. Magnetic
 25 characterization was collected using Vibrating Sample Magnetometry (VSM) on a Quantum Design Versalab physical property measurement system. Measurements were collected in fields from 3 Tesla to -3 Tesla and temperatures from 50 K to 300 K. Honda-Owen plots were constructed from collected
 30 magnetization vs. applied field data to quantify the amount of paramagnetic susceptibility.¹⁶

Results

The initial reaction mixtures of oleylamine and 3-EG or 4-EG
 35 were a translucent yellow/golden color at 300 °C. A reaction temperature of 300 °C was chosen to remain below the decomposition temperature of the nanocrystalline Co₃C and Co₂C phases.⁸ Upon addition of the cobalt precursor the solution turned purple indicative of dissolution of the cobalt nitrate
 40 precursor. Within less than a minute, the solution transitioned to a dark green, opaque color, regardless of whether 3-EG or 4-EG was used. A dark green solution is commonly observed when using high boiling amines for the synthesis of cobalt oxide (CoO) with a hexagonal crystal structure.^{17, 18} As the reaction
 45 progressed, the dark green solution converted to a dark brown solution.

XRD analysis for short reaction times using a mixture of 4-EG and oleylamine revealed cobalt oxide (CoO) particles to form, possessing the hexagonal, wurtzite structure (space group
 50 P63/mmc). The formation of hexagonal CoO is in agreement with the color change from a purple to a dark green solution, shortly after addition of the cobalt precursor.^{17, 18} With increasing reaction times the crystal phase transitioned from CoO to Co₂C (Figure 1(a)). After 4 hours, the particle mixture was comprised
 55 of 87.9% Co₂C. Working at 300 °C the transition of CoO to Co₂C showed nearly a linear progression as shown in Figure 1(b). Interestingly, at no time interval were peaks consistent with a metallic cobalt phase detected. This implies that reduction of CoO and Co₂C formation occurs with no formation of an
 60 intermediate crystalline metallic cobalt phase. Crystal grain sizes

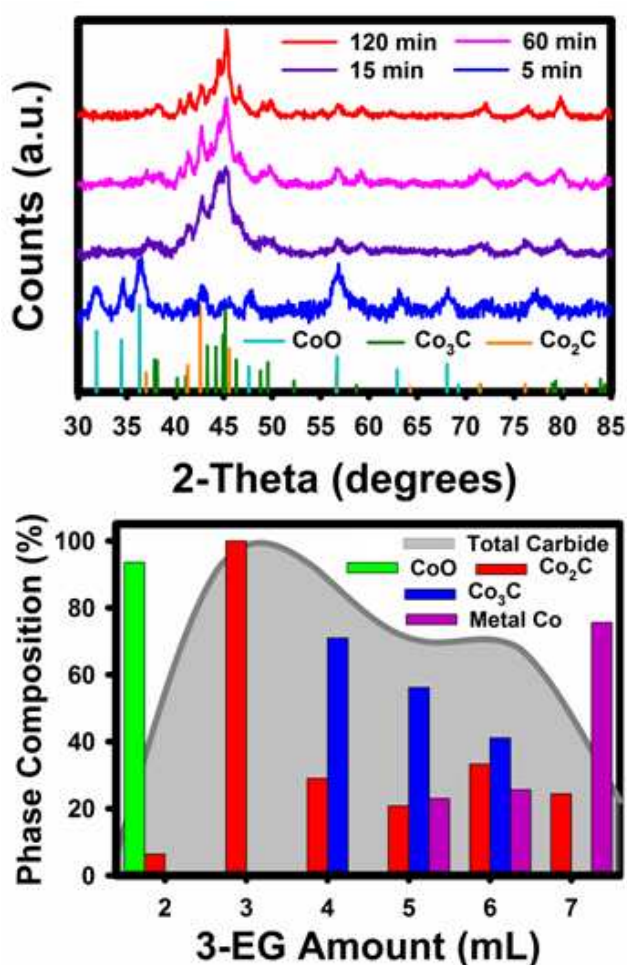


Figure 2. (a) XRD scans collected for different reaction times. Stick plots for CoO, Co₂C and Co₃C are shown below, for reference. (b) Bar graph showing the phase composition for reactions run at varying 3-EG amounts. Individual scans can be seen in Supplemental Information (S2).

of 12 nm for CoO and 10 nm for Co₂C were calculated for samples at each reaction time when using a 10:15 ratio of 4-EG to oleylamine. However, changing the ratio of 4-EG to oleylamine significantly altered the phase and crystal grain sizes formed (Figure 1(c)).

Syntheses ran in the absence of 4-EG resulted in only cobalt oxide phases being identified through XRD analysis. At a 15 minute reaction time, CoO crystals 35 nm in diameter were produced. Increasing the reaction time to 2 hours, showed an increase in crystal grain size for CoO to 65.8 nm, however no peak intensities consistent with Co₂C were observed. Adding 2.5 mL of 4-EG to the reaction system resulted in the formation of a mixture of 58.8% CoO and 42.2% Co₂C. The calculated crystal grain sizes for CoO and Co₂C phases were 49.3 nm and 12.6 nm, respectively. Syntheses conducted using 5, 10, and 15 mL of 4-EG produced consistent phase ratios and crystal grain sizes (Figure 1(c)). Grain sizes for CoO and Co₂C were between 10-15 nm, and Co₂C compositions fell between 50-60 % in this 4-EG volume range. Increasing to 20 mL of 4-EG led to a decrease in Co₂C phase percent, as well as a decrease in the calculated crystal grain size to 8 nm. The changes in crystal phase and crystal grain size, even at low amounts of 4-EG, shows that the addition 4-EG

leads to reduction and carbide formation, where oleylamine by itself does not. The addition of 4-EG also plays a significant role determining the grain size of the formed CoO and Co₂C crystals.

Exchanging 4-EG for 3-EG led to an overall increase in the kinetics of carbide formation, along with inducing the formation of the Co₃C phase. As is shown in Figure 2(a), crystalline CoO phases were the majority phase present 5 minutes after addition of the cobalt precursor. Within 15 minutes after addition, peak intensities and peak positions consistent with Co₃C and Co₂C phases could be identified. However peak resolution was poor, implying poor crystallinity or small crystal grain sizes. As the reaction progressed, the diffraction peaks narrowed and intensified, indicative of improved crystallinity. At a reaction time of two hours, all peaks could be indexed to the Co₃C and Co₂C phases. The phase composition was calculated to be 71% Co₃C and 29% Co₂C when using 4 mL of 3-EG. As was shown with 4-EG, varying the amount of 3-EG could be used to alter crystal phase ratios.

At low volumes of 3-EG (2 mL) the majority phase produced was CoO, very similar to the results when using small volumes of 4-EG. Increasing the amount of 3-EG saw the synthesis of pure phase Co₂C at 3 mL of 3-EG, and a biphasic product of Co₂C and Co₃C at 4 mL of 3-EG. At 3-EG volumes greater than 4 mL, peak intensities consistent with metallic cobalt phases could be indexed. At a 3-EG volume of 7 mL, 75% of the crystalline phase composition were fit to metallic cobalt phases. Calculated phase ratios for syntheses conducted at varying 3-EG volumes is shown in Figure 2(b). Grain sizes for the Co₂C and Co₃C phases were calculated to be between 15-20 nm, in most cases. The grain size for metallic Co in the reaction containing 7 mL of 3-EG was calculated to be 8 nm. The XRD analysis shows that interchanging 3-EG and 4-EG causes the formation of Co₃C and increases the reduction and carbide formation rates. However, this influence extends beyond the crystallographic properties and kinetics of formation, but also causes variance in particle morphology.

In syntheses containing 4-EG and oleylamine, spherical particles averaging 200-400 nm in diameter were formed (Figure 3(a)). Inspection of the particle surface revealed the presence of small anisotropic primary particles that are 10 nm in diameter and greater than 15 nm in length (Figure 3(b)). The diameter of these small primary particles is consistent with crystal grain sizes calculated from XRD. The formation of large, spherical secondary particles comprised of small primary crystallites is common for polyol synthesized Co_xC particles.^{6, 8} In many cases, dimers and trimers of secondary particles were observed, as shown in Figure 3(c). These dimers and trimers exhibited large, low density interfacial regions. At long reaction times (e.g. 4 hours) many hollow spheres (Figure 3(d)) and large rod-like agglomerations of the spherical secondary particles existed (Supplemental S3). Comparing particle contrast as a function of reaction time revealed particles of varying contrast at short reaction times (Figure 3(a)); long reaction times produced darker denser structures. FT-IR spectra of synthesized particles showed a decrease in carbonaceous residue with increased reaction times (Supplemental S8). Hence, the increased particle contrast at longer reaction times can be attributed to a decrease in carbonaceous residue from the secondary structures. The loss of

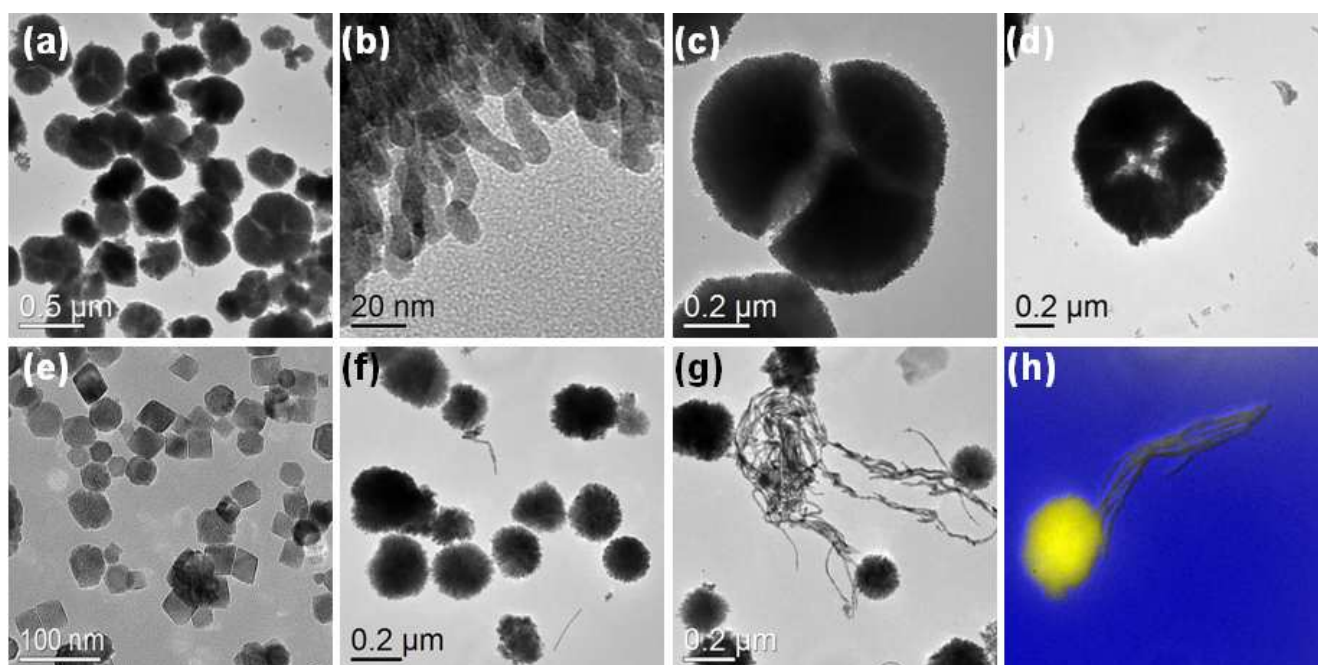


Figure 3. TEM Images of particles synthesized in a 10 mL and 15 mL of oleylamine mixture at (a-c) short reaction times (0.25-1 hour) and (d) extended reaction times (e.g. 4 hours). (e) CoO particles synthesized in oleylamine. (f,g) Co₂C and CoO particles synthesized using 2.5 mL of 4-EG. (h) EELS map of Co L-edge, with cobalt shown in yellow.

5 carbonaceous residue also helps explain the formation of hollow spherical secondary particles at prolonged reaction times.

Particles synthesized in oleylamine, without the addition of 4-EG, resulted in a drastic change in particle morphology. Polydispersed cubes and spheres of 30-40 nm diameter cobalt oxide, were observed (Figure 3(e)), which is consistent with previous reports using high boiling point amines as a solvent and surfactant for the synthesis of CoO particles.¹⁸ However, adding just 2.5 mL of 4-EG resulted in the formation of the several hundred nanometers in diameter secondary particles. Many long 1-D structures were interwoven amongst the particles synthesized in low amounts of 4-EG (Figure 3(g)). EELS mapping showed the 1-D structures to contain cobalt (Figure 3(h)). Dark field imaging confirmed the presence of small cobalt crystallites to be embedded in the tubes, in some instances (Supplemental S3). Collected Raman spectra did not show significant signal for the D and G bands of carbon (Supplemental S). Hence, it is unclear the nature of these 1-D at this time.

Particles synthesized in 3-EG show secondary structures 200-300 nm diameter comprised of smaller nanocrystals, very similar size and morphology to those synthesized in 4-EG (Figure 4). However at short reaction times (e.g. 5 minutes), a dense carbonaceous matrix coated the particles and caused a high degree of agglomeration to occur (Figure 4(a,b)). At 15 minutes, a dramatic decrease in this surface organic layer was observed (Figure 4(c)). The smaller crystallites present on the surface of the particles appeared as long rod-like projections 7-10 nm in diameter, but still possessed a 3-5 nm organic capping layer (Figure 4(d)). This capping layer is commonly observed in solution synthesized Co_xC particles.⁶⁻⁸ Long reaction times (e.g. 2 hours) showed no change in the morphology of the spherical secondary particles but the smaller surface primary particles possessed increased diameters and decreased aspect ratios. The

increase in size of the surface primary particles is in good agreement with the decrease in peak width/ increase in crystal grain size that is observed in XRD.

While increased reactions times showed a decrease in surface organic residue on the particles surface, an increase in amorphous carbon content was observed. Raman spectra showed an increase in the D and G band signal of carbon (1355 cm⁻¹ and 1575 cm⁻¹, respectively) with increasing reaction time. Peaks for cobalt oxide and adsorbed N₂ were also identified at 682 cm⁻¹ and 2330 cm⁻¹, respectively. The trend of increased carbon formation in Raman spectra agrees well with the increase in carbide formation seen in XRD spectra. However, the lack of D and G band signal at a 5 minute reaction time points towards the dense organic surface layer witnessed in TEM images (Figure 4(a,b)) to not be amorphous carbon. Hence, the chemical reactions coinciding to the decomposition of this organic surface layer and leading to the formation of amorphous carbon and cobalt carbide were further investigated.

To monitor the chemical reactions occurring in the reaction mixture during synthesis, FT-IR spectra were analyzed for aliquots collected at various reaction times. Initially adding a glycol to the oleylamine caused a decrease in the intensity of the N-H bend peak at 792 cm⁻¹ of the oleylamine. This implies that the glycols have an impact on the hydrogen bonding of the reaction mixture. After addition of the cobalt precursor at 300 °C, the NH₂ scissoring absorption at 1600 cm⁻¹ showed diminished intensities with increasing reaction time, while a new peak at 1670 cm⁻¹ emerged (Figure 5(a)). The new peak at 1670 cm⁻¹ is consistent with the C=N stretch of an imine functionality.¹⁹ A peak at 1647 cm⁻¹, consistent with a C=C stretching mode was consistent throughout the reaction, implying that the unsaturated hydrophobic tail of the oleylamine is unaffected during the reaction process. Concurrent with the emergence of the imine

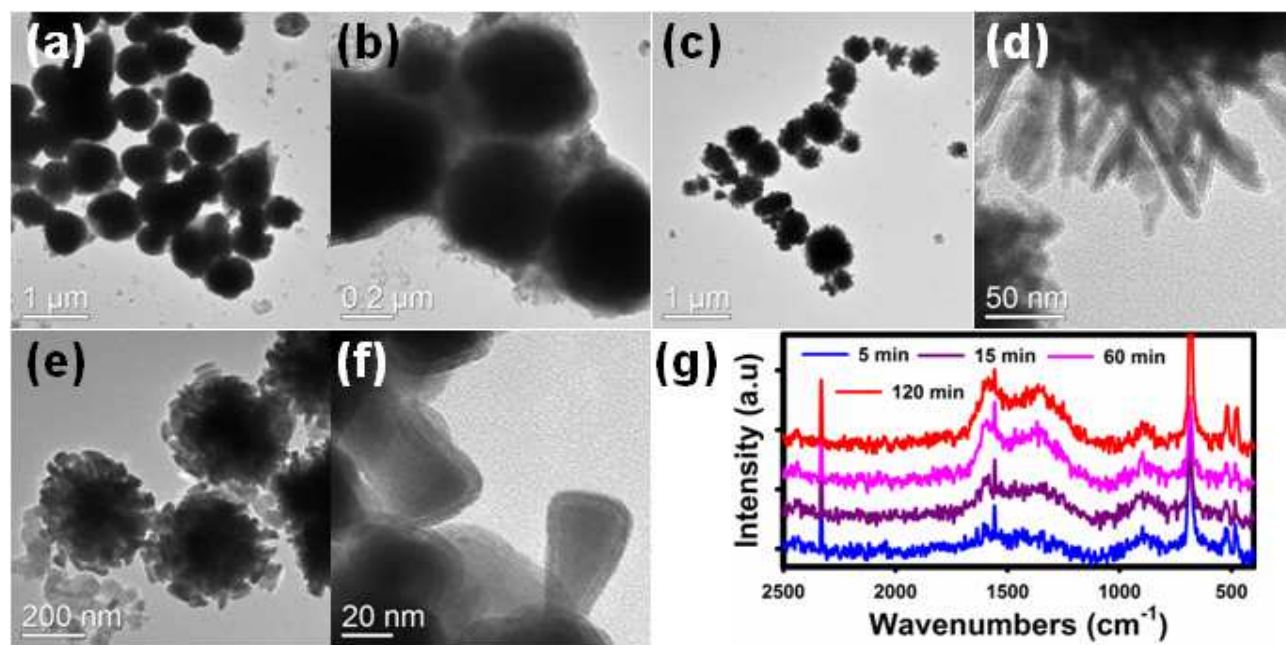


Figure 4. TEM images of particles synthesized with 5 mL of 3-EG in 20 mL of oleylamine at (a,b) 5 minute (c,d) 15 minute, and (e,f) 2 hour reaction times. (g) Raman spectra of Co_xC particles collected at various reaction times.

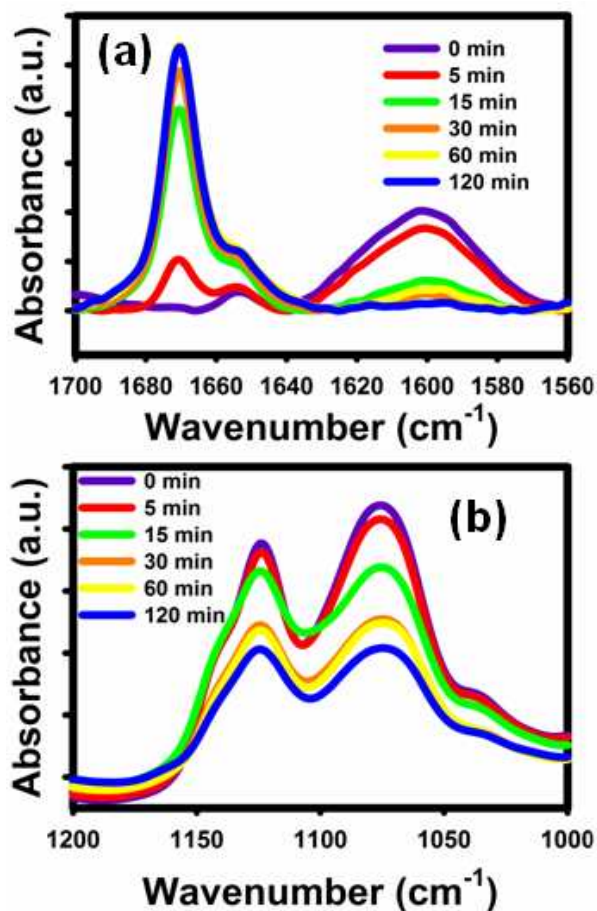


Figure 5. FT-IR Spectra in the wave number range of (a) 1560-1700 and cm^{-1} (b) 1000-1200 cm^{-1} , for samples of the reaction mixture at various reaction times.

peak at 1670 cm^{-1} , a decrease in peaks at 1120 cm^{-1} and 1070 cm^{-1} was observed (Figure 5(b)), consistent with the stretching
 10 modes of ether (C-O-C) bonds. Possible mechanisms for the formation of an imine and its correspondence to the loss of ether bonds will be addressed in the Discussion section.

Co_2C is ferromagnetic at room temperature and possesses high magnetocrystalline anisotropy, resulting in hard ferromagnetic
 15 properties.⁶⁻⁸ For pure Co_2C nanostructures, magnetic saturation values of as high as 15 emu/g and coercivities up to 1.2 kOe have been reported.⁷ In this study, $\text{Co}_2\text{C}/\text{CoO}$ samples synthesized in
 4-EG showed magnetization values between 2-5 emu/g. A magnetization vs. applied field ($M(H)$) curve for a sample
 20 containing 87.9% Co_2C is shown in Figure 6(a). CoO is paramagnetic at room temperature and antiferromagnetic at low temperatures. Hence, the lower magnetization values for the
 $\text{Co}_2\text{C}/\text{CoO}$ nanostructures when compared to literature can be attributed to a weight dilution from the
 25 paramagnetic/antiferromagnetic CoO . The $\text{Co}_2\text{C}/\text{CoO}$ samples showed an increase in coercivity values at temperatures from 50 K to 300 K with increasing Co_2C amount (Figure 6(b)).

Formation of the Co_xC phase when using 3-EG resulted in increased magnetization and coercivity values over those
 30 synthesized using 4-EG. In Figure 7(a), the magnetic properties as a function of reaction time can be seen for the 3-EG system. At 5 minutes, low magnetizations and low coercivities are observed,
 commensurate with the formation of CoO phases seen in XRD. Increasing reaction times to 15 minutes, results in a dramatic
 35 increase in magnetization values and a slight increase in coercivity. This can be explained by the transition of paramagnetic CoO to ferromagnetic Co_xC phases. Above a 15 min reaction time magnetization values remained constant but a
 steady increase in coercivity values occurred. The increase in
 40 coercivity can be attributed to increased crystallinity and larger crystal grain sizes which is confirmed by a narrowing of XRD

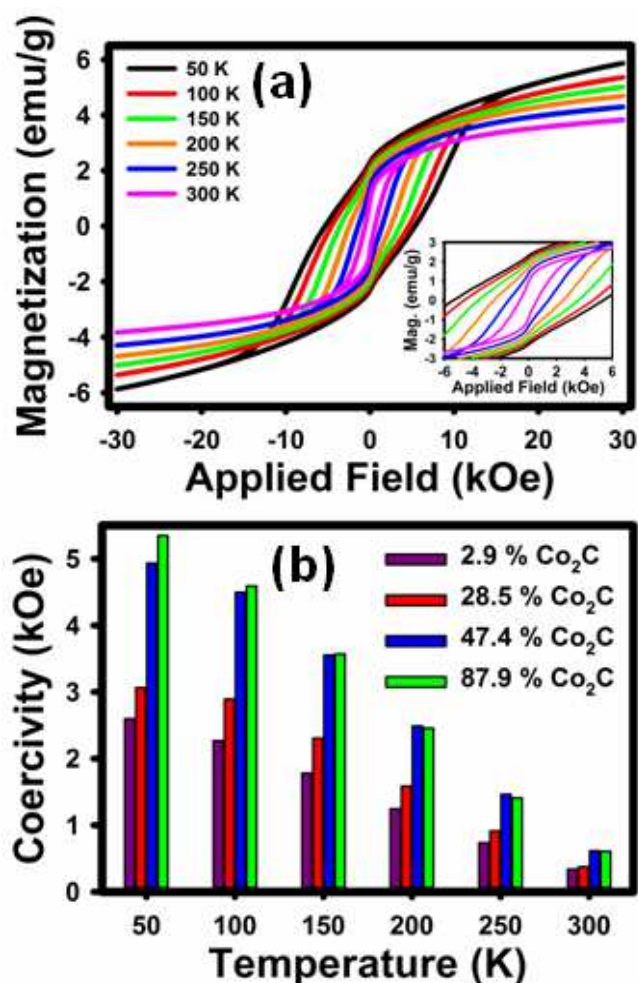


Figure 6. (a) Magnetization vs. applied field curves at various temperatures for Co₂C/CoO particles. (b) Coercivity values at various temperatures for particles of varying Co₂C composition.

peaks with increased reaction times (Figure 2(a)). The magnetic properties as a function of [3-EG] can be seen in Figure 7(b). The highest coercivity values were observed in samples containing a mixture of Co₂C and Co₃C phases. The presence of metal Co phases caused an increase in magnetization values but a decrease in coercivity values.

Discussion

Polyethylene glycols like 4-EG and 3-EG can readily undergo thermo-oxidation above 70 °C in an oxygen containing atmosphere.^{13, 20-22} This thermo-oxidation causes a cleavage of the terminal carbon-carbon bond producing formic acid as an oxidation product. The formic acid can react with the other glycol molecules to form formyl esters. On the other hand, ethylene glycol oxidizes to glycolaldehyde in the presence of atmospheric oxygen.²³ In studies probing the reduction of transition metals by ethylene glycol, the rate of glycolaldehyde formation was strongly correlated to the rate of reduction and formation of metal nanoparticles.^{12, 23} In the current study, no peaks consistent with formic acid or a formyl ester were observed in collected FT-IR spectra of the reaction solution. The identification of imine functionality does support the oxidation of the glycol to an

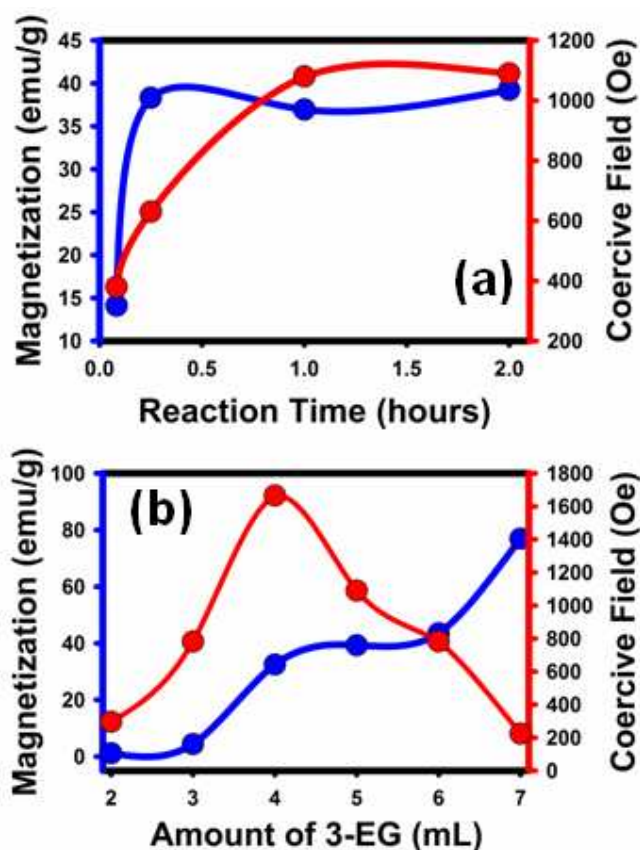


Figure 7. (a) Magnetic properties as a function of time for particles synthesized in 5 mL of 3-EG at various times. (b) Magnetic properties as a function of 3-EG volume for 2 hour reaction time.

aldehyde (Figure 5(a)). Primary amines, like oleylamine, can be used as indicators for the presence of trace amounts of carbonyl containing compounds through the reaction of an amine and aldehyde to form an imine and water.^{12, 23} Therefore, the rate of imine formation can be used to assess the rate of glycol oxidation. Intensities for the imine peak prior to addition of the cobalt precursor were not detected; implying that oxidation of the glycol is slow in the absence of oxygen or cobalt. However, after addition of the cobalt nitrate precursor, a dramatic increase in glycol oxidation rate was observed (Figure 8(a)). While the initiation of glycol oxidation seemed to be dependent upon the addition of the cobalt precursor, large variances in the extent of glycol oxidation arose for reactions ran at different glycol amounts. The highest rates of imine formation occurred in reactions with 3 mL and 4 mL of 3-EG, which yielded particles comprised of 100% carbide phases (Figure 8(a)). For reactions with low imine formation rates, either CoO or Co metal impurity phases were identified through XRD analysis. From a crystallographic standpoint, the dramatic increase in the amount of glycol oxidation in the 0-15 reaction time range is commensurate with the observance of CoO undergoing reduction and formation of Co_xC phases (Figure 2(a)). The reduction of CoO is one obvious source of glycol oxidation to an aldehyde, but this does not fully explain the correlation between high glycol oxidation rates and Co_xC phase formation. One explanation could be that a fast reduction process of the CoO phases is necessary to allow for complete carbon diffusion and lattice

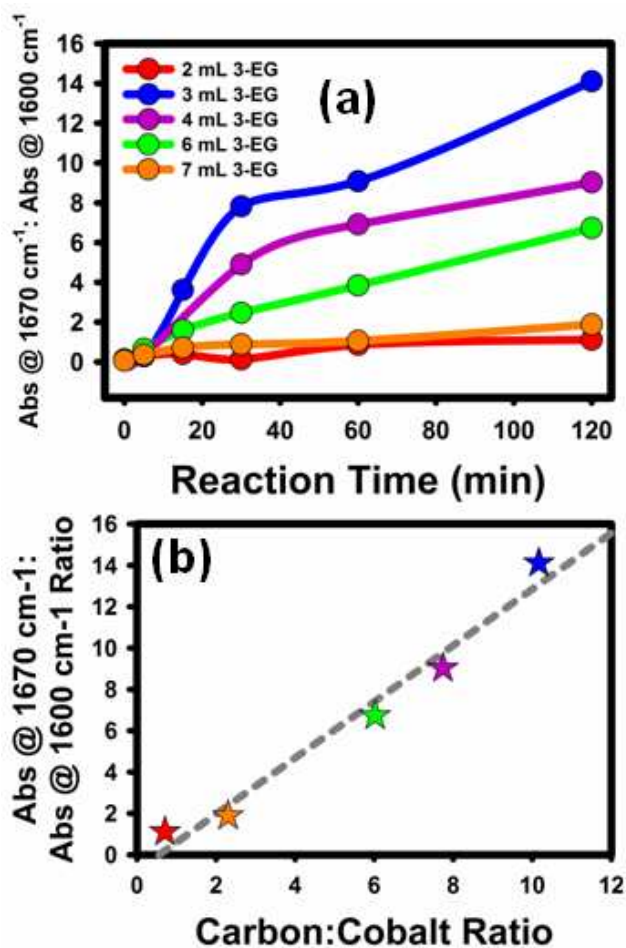


Figure 8. (a) Comparison of the rate of imine formation for various amounts of 3-EG as a function of time. (b) Comparison of intensity of imine peak observed in FT-IR spectra versus amount of carbide phase formed for particles synthesized in 3-EG.

reconstruction. However, the possibility that the oxidized form of the glycol acts as a carbon source, promoting the formation of Co_xC phases cannot be ruled out.

While the rates of glycol oxidation are strongly correlated to the amount of 3-EG in the solvent mixture, changing from 3-EG to 4-EG also affects the rate of glycol oxidation. When using 4-EG as opposed to 3-EG, the transition from oxide to carbide occurred at a much slower rate. Nearly pure crystalline cobalt carbide phases could be seen in as little as 15 minutes after addition of the cobalt precursor, in 3-EG. In 4-EG it took as long as 4 hours to reach 90% pure Co_2C , with CoO as the remaining impurity phase. The trends for measured oxidation rates correspond well with a decrease in carbonaceous material as witnessed in the TEM images and FT-IR spectra for particles in Figure 3 and Figure 4 (FT-IR in Supplemental S8). Particles synthesized in 3-EG (Figure 4) showed a dramatic decrease in surface carbonaceous residue present on the particles surface between 5-15 minute reaction times. However when using 4-EG, a decrease in the organic content within the particles was only witnessed at 4 hour reaction times, where hollow spheres were observed to form (Figure 3(d)). This change in rate can be attributed to the difference in boiling points between 3-EG and 4-

EG. Maintaining a constant reaction temperature of 300 °C meant that reactions with 3-EG were conducted above its boiling point (BP=285 °C). 4-EG has a boiling point of 327 °C, and leads to lowered reactivity and a slower rate of oxidation. Hence, the glycol's boiling point, oxidative stability, and amount used are key parameters that need to be taken into account to achieve the synthesis of pure phase Co_xC nanoparticles.

Conclusions

In conclusion, we report a versatile approach to the synthesis of Co_xC , Co metal, and CoO based nanocomposites. By using the polyol process, kinetics and crystal phase can be controlled by using polyols of varying ethylene glycol monomer units. Using a mixture of 4-EG and oleylamine led to a slow transition from CoO to Co_2C based materials. Switching to 3-EG allowed for the synthesis of CoO, Co_2C , Co_3C , and Co particles, dependent on the amount of 3-EG used. Syntheses ran in the absence of 4-EG or 3-EG resulted in the formation of only CoO phases, implying the glycols to be the source of reduction and carbon atoms. Along with the glycol used, the amount of carbide formed was shown to be strongly correlated to the rate of oxidation of the glycol, with the highest rates of oxidation leading to pure Co_xC particles. This simple approach of tuning the kinetics and crystal phase formed, through proper selection of reactants used for the synthesis of Co_xC based materials, can allow for proper control of the magnetic properties and helps to further understand the mechanism for the solution based synthesis of Co_xC based nanomaterials. The conclusions section should come at the end of article.

Acknowledgements

Financial support from the ARPA-e REACT program 1574-1674 is greatly acknowledged. The help of the staff of the VCU Nanomaterials Core Characterization Facility is also greatly appreciated. This work was also partially funded through a graduate research fellowship through Altria Group Inc.

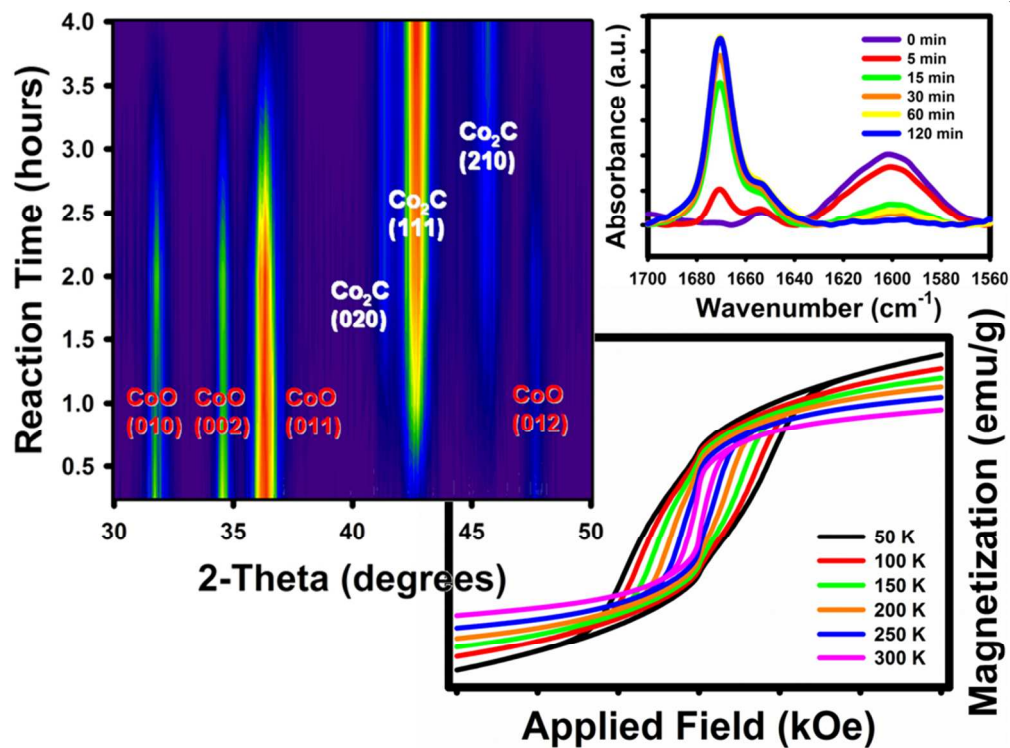
Notes and references

*Virginia Commonwealth University, Department of Chemistry, 1001 W. Main Street, Richmond, Va USA.; E-mail: ecarpenter2@vcu.edu

† Electronic Supplementary Information (ESI) available: Individual XRD patterns, Raman spectra, FT-IR spectra and TEM images are included. See DOI: 10.1039/b000000x/

1. E. Iglesia, Appl. Catal. A-Gen., 1997, 161, 59-78.
2. K. J. Strnat and R. M. W. Strnat, Journal of Magnetism and Magnetic Materials, 1991, 100, 38-56.
3. T. Maurer, F. Ott, G. Chaboussant, Y. Soumare, J. Y. Piquemal and G. Viau, Applied Physics Letters, 2007, 91.
4. Y. Soumare, C. Garcia, T. Maurer, G. Chaboussant, F. Ott, F. Fievet, J. Y. Piquemal and G. Viau, Advanced Functional Materials, 2009, 19, 1971-1977.
5. G. Viau, C. Garcia, T. Maurer, G. Chaboussant, F. Ott, Y. Soumare and J. Y. Piquemal, Physica Status Solidi a-Applications and Materials Science, 2009, 206, 663-666.
6. V. G. Harris, Y. Chen, A. Yang, S. Yoon, Z. Chen, A. L. Geiler, J. Gao, C. N. Chinnasamy, L. H. Lewis, C. Vittoria, E. E. Carpenter, K. J. Carroll, R. Goswami, M. A. Willard, L. Kurihara, M. Gjoka and O. Kalogirou, Journal of Physics D-Applied Physics, 2010, 43, 7.
7. Z. J. Huba and E. E. Carpenter, J. Appl. Phys., 2012, 111, 07B529.

8. K. J. Carroll, Z. J. Huba, S. R. Spurgeon, M. Qian, S. N. Khanna, D. M. Hudgins, M. L. Taheri and E. E. Carpenter, *Applied Physics Letters*, 2012, 101, 012409.
9. F. Fievet, J. P. Lagier, B. Blin, B. Beaudoin and M. Figlarz, *Solid State Ionics*, 1989, 32-3, 198-205.
10. N. Chakroune, G. Viau, C. Ricolleau, F. Fievet-Vincent and F. Fievet, *Journal of Materials Chemistry*, 2003, 13, 312-318.
11. T. Hinotsu, B. Jeyadevan, C. N. Chinnasamy, K. Shinoda and K. Tohji, *J. Appl. Phys.*, 2004, 95, 7477-7479.
- 10 12. R. J. Joseyphus, T. Matsumoto, H. Takahashi, D. Kodama, K. Tohji and B. Jeyadevan, *Journal of Solid State Chemistry*, 2007, 180, 3008-3018.
13. A. M. Sakharov, L. I. Mazaletskaya and I. P. Skibida, *Kinetics and Catalysis*, 2001, 42, 662-668.
- 15 14. L. Q. Wang, H. Meng, P. K. Shen, C. Bianchini, F. Vizza and Z. D. Wei, *Physical Chemistry Chemical Physics*, 2011, 13, 2667-2673.
15. W. B. Pearson, *Handbook of Lattice Spacings and Structures of Metals*, Pergamon Press, London, 1967.
16. K. Honda, *Annalen Der Physik*, 1910, 32, 1027-1063.
- 20 17. K. An, N. Lee, J. Park, S. C. Kim, Y. Hwang, J. G. Park, J. Y. Kim, J. H. Park, M. J. Han, J. J. Yu and T. Hyeon, *Journal of the American Chemical Society*, 2006, 128, 9753-9760.
18. K. M. Nam, J. H. Shim, D. W. Han, H. S. Kwon, Y. M. Kang, Y. Li, H. Song, W. S. Seo and J. T. Park, *Chemistry of Materials*, 2010, 22, 4446-4454.
- 25 19. A. Meffre, S. Lachaize, C. Gatel, M. Respaud and B. Chaudret, *Journal of Materials Chemistry*, 2011, 21, 13464-13469.
20. J. N. Hemenway, T. C. Carvalho, V. M. Rao, Y. M. Wu, J. K. Levons, A. S. Narang, S. R. Paruchuri, H. J. Stamato and S. A. Varia, *J. Pharm. Sci.*, 2012, 101, 3305-3318.
- 30 21. J. Glastrup, *Polymer Degradation and Stability*, 1996, 52, 217-222.
22. Y. Kitahara, S. Takahashi and T. Fujii, *Chemosphere*, 2012, 88, 663-669.
- 35 23. S. E. Skrabalak, B. J. Wiley, M. Kim, E. V. Formo and Y. N. Xia, *Nano Letters*, 2008, 8, 2077-2081.



By changing the polyhydric alcohol and reaction time, the cobalt crystal phase can be manipulated and allow for control of the resulting magnetic properties.

271x202mm (96 x 96 DPI)